Observation and analysis of multiple dark-antidark solitons in two-component Bose-Einstein condensates

G. C. Katsimiga,[1] S. I. Mistakidis,[1] T. M. Bersano,[2] M. K. H. Ome,[2] S. M. Mossman,[2] K. Mukherjee,[1,3] P. Schmelcher,[1,4] P. Engels,[2] and P. G. Kevrekidis[5,6]

[1]*Department of Physics, Center for Optical Quantum Technologies, University of Hamburg, Luruper Chaussee 149, 22761 Hamburg, Germany*

[2]*Department of Physics and Astronomy, Washington State University, Pullman, Washington 99164-2814, USA*

[3]*Indian Institute of Technology Kharagpur, Kharagpur-721302, West Bengal, India*

[4]*The Hamburg Centre for Ultrafast Imaging, University of Hamburg, Luruper Chaussee 149, 22761 Hamburg, Germany*

[5]*Department of Mathematics and Statistics, University of Massachusetts Amherst, Amherst, Massachusetts 01003-4515, USA*

[6]*Mathematical Institute, University of Oxford, Oxford OX26GG, United Kingdom*

(Received 29 February 2020; accepted 11 June 2020; published 3 August 2020)

We report on the static and dynamical properties of multiple dark-antidark solitons (DADs) in two-component, repulsively interacting Bose-Einstein condensates. Motivated by experimental observations involving multiple DADs, we present a theoretical study which showcases that bound states consisting of dark (antidark) solitons in the first (second) component of the mixture exist for different values of interspecies interactions. It is found that ensembles of few DADs may exist as stable configurations, while for larger DAD arrays, the relevant windows of stability with respect to the interspecies interaction strength become progressively narrower. Moreover, the dynamical formation of states consisting of alternating DADs in the two components of the mixture is monitored. A complex dynamical evolution of these states is observed, leading either to sorted DADs or to beating dark-dark solitons depending on the strength of the interspecies coupling. This study demonstrates clear avenues for future investigations of DAD configurations.

DOI: 10.1103/PhysRevA.102.023301

I. INTRODUCTION

Over the past 25 years, the experimental implementation of dilute-gas Bose-Einstein condensates (BECs) has provided a fertile platform for the exploration of a wide range of macroscopic quantum features [1–3]. One of the major axes around which this effort has revolved is the study of nonlinear waves and their existence, dynamics, and interactions within this atomic physics platform [4]. Such waves were previously recognized as playing a substantial role in other fields including nonlinear optics [5], as well as water waves [6]. The realm of atomic BECs, however, has enabled the study of a wide range of such patterns including, but not limited to, dark solitons [7], vortical states [8–10], and also more complex entities such as hopfions [11] and even vortex knots [12,13].

Beyond the setting of single-component atomic condensates (which have been the focus of many of the above studies), recent efforts have considered multicomponent generalizations of soliton formation and dynamics [14]. A fundamental state of interest has been the dark-bright (DB) solitary wave and its close relative, the dark-dark solitary state [15–21]. While the relevance of this state to the dynamics of multiple polarizations of light in photorefractive crystals was originally recognized early on in pioneering works in nonlinear optics [22,23], it was not until their proposal [24] and especially first experimental realization [25] in atomic BECs that an explosion of interest ensued [26–31]. In recent years, this direction of research has gained further momentum through the study of variants of solitary waves such as nonlinear polarization waves [32] and magnetic solitons [33], so-called dark-antidark (DAD) structures (where antidark means a bright solitonic state on top of a finite background) [34], and extensions to spinor (three-component) solitary waves [35]. This thrust continues intensely through both experimental and theoretical studies; see, e.g., Ref. [36] for a recent synthesis.

In an earlier work, we reported the possibility of an experimental realization of DAD structures [34], as indicated above. The experimental efforts described in the present work showcase the generation of multiple such structures in two different formats: we have observed settings in which the (multiple) dark solitons are all in the same component and the antidark solitons are all in the second component, as well as ones where there is an alternating sequence of darks and antidarks (in a complementary fashion) between the two components. This, in turn, motivates a theoretical study of each one of these two configurations of multi-dark-antidark solitons. On the one hand, this investigation naturally extends the setting of a single dark-antidark soliton [34], while on the other hand, it complements studies of multiple dark-bright solitons [28,37] and even multiple dark solitons [4]. The key result is that states in which all dark solitons are contained in one component and antidarks in the other can be dynamically robust for a few dark-antidark solitons (DADs), but become progressively less stable for more DADs, in line with experimental observations. Also in agreement with experiment, alternating DAD states (where, for instance, in each component a dark soliton is neighboring two antidark solitons, and vice versa) are not found as stationary solutions,

but only as dynamical states in the two-component systems considered. The dynamics of both types of states is explored.

Our presentation is structured as follows. In Sec. II, we present the experimental demonstration of the corresponding states as they are generated in our two-component experiments with ^{87}Rb BECs. Section III describes the modeling platform of the relevant system, while in Sec. IV we analyze the existence, stability, and dynamics of the different multisoliton DAD states obtained in the context of the theoretical model. In Sec. V, we briefly discuss the dynamical evolution of configurations consisting of few alternating DADs. Finally, we summarize our findings and present our conclusions as well as some directions for future studies in Sec. VI.

II. EXPERIMENTAL DEMONSTRATION

To motivate our investigation of multisoliton DAD states, we begin by showcasing experimental results demonstrating the creation and stability of such structures. To experimentally realize an arrangement of DAD solitons, we employ a procedure based on Rabi winding [38,39]. An elongated BEC of approximately 4.5×10^5 ^{87}Rb atoms is prepared in the $|F, m_F\rangle = |1, -1\rangle$ hyperfine state, optically confined by a single-beam dipole trap with trap frequencies of approximately $\{\omega_x, \omega_y, \omega_z\} = 2\pi\{1.5, 140, 180\}$ Hz. The weakly confined x axis is oriented horizontally.

We apply an external magnetic field of approximately 1 G with a linear gradient of approximately 5 mG/cm along the long axis of the BEC. This produces a spatially varying Zeeman shift within the $F = 1$ and $F = 2$ hyperfine manifolds. A uniform, fixed-frequency microwave (MW) field is used to drive transitions between the $|1, -1\rangle$ and $|2, -2\rangle$ states. In the following, we consider these two states as the pseudospin orientation of a spin-1/2 system. The two-level Rabi formula for the population of atoms in the $|2, -2\rangle$ level, $P_{|2,-2\rangle}$, takes a spatially dependent form [40] given by

$$P_{|2,-2\rangle}(x,t) = \frac{\Omega^2}{\Omega^2 + \delta^2(x)} \sin^2\left[\frac{\sqrt{\Omega^2 + \delta(x)^2}}{2} t\right], \qquad (1)$$

where Ω is the resonant Rabi frequency, t is the winding time, and δ is the detuning of the microwave coupling which varies across the cloud due to the spatially dependent Zeeman shift. By applying the microwave drive for a given amount of time, a magnetization pattern is created in the condensate corresponding to the phase winding caused by the differential Rabi cycling. The magnetic field gradient is then suddenly removed and the BEC is allowed to evolve in the now homogeneous magnetic field. The resulting dynamics are observed by turning off the optical trap and selectively imaging the two hyperfine states sequentially after 15 ms (17 ms) of time of flight for the $|2, -2\rangle$ ($|1, -1\rangle$) state. Our imaging technique allows us to image both states in each experimental run. There is negligible evolution occurring in the time between the two exposures taken for each run, so that features in the two states can be accurately superimposed to represent the in-trap spin structure of the state. Figure 1 presents a variety of these absorption images where the $|2, -2\rangle$ state is on top and the $|1, -1\rangle$ is at the bottom, followed by integrated cross sections corresponding to the absorption image above.

For a MW driving frequency that is close to the resonance frequency at the center of the atom cloud, a high-amplitude winding pattern results. Figure 1(a) shows a state produced after 15 ms of Rabi winding with $\Omega/2\pi = 19$ kHz. The population of the two (pseudo)spins alternates along the elongated direction of the BEC with a large amplitude. Looking at Fig. 1, it is important to reiterate that the two spin components are imaged separately while the cloud falls, but the dynamics we describe here occur in the optical trap where the two spin components exist together. The bright features in one spin component fill the dark regions of the other spin component in this case. After 150 ms of evolution in the optical trap, which is a long time on the scale of mean-field effects but a short time in terms of the x-axis trap frequency, a regular array of alternating DAD solitons corresponding to the initial winding appears [see Fig. 1(b)]. The DAD solitons are characterized by a dark notch of low density in one component, which is filled in by a bright stripe of high density in the other component. These features are distinct from DB solitons in that the bright component exists on a finite background density which does not go to zero. After allowing these solitons to evolve in the trap for 450 ms, which is longer than half of a trap period, Fig. 1(c) shows that the arrangement has broken into an irregular collection of solitonic features and domains rather than a regular array of alternating DAD solitons. One can clearly discern some well-defined features with widths characteristic of dark solitons [41], but the regular pattern demonstrated in Fig. 1(b) does not persist.

Alternatively, a MW driving frequency which is farther detuned from resonance will produce an array of spin-mixed regions separated by regions of spin purity, as described by Eq. (1) when the detuning δ varies linearly with a large offset. Figures 1(d)–1(f) show the spin populations after an identical winding procedure to that describing Figs. 1(a)–1(c), and for same time increments, but with a microwave frequency 11 kHz detuned from the resonant frequency at the center of the cloud. Here, the partial spin transfer only allows dark solitons to form in the $|2, -2\rangle$ component. After approximately 250 ms of evolution time following the MW winding, collections of DADs start to nucleate, leading to persistent configurations containing between two and four DAD solitons in clusters, as shown in Fig. 1(f). Figure 1(f) shows density notches in the $|2, -2\rangle$ component with the width characteristic of dark solitons in this system, and there are corresponding high-density regions in the other spin state. While we observe density depressions in the second component ($|1, -1\rangle$) between the antidark solitons, these depressions are of a larger length scale than the characteristic soliton scale and are therefore more appropriately interpreted as a reduced background density for the antidark solitons. These clusters are unique to the nonalternating (alias sorted) DAD configurations, i.e., those with all the dark features in one component and bright features in the other, and therefore motivate a detailed investigation of the conditions under which stable DAD configurations can form.

III. THEORETICAL FRAMEWORK

Motivated by the experimental observations of Sec. II, we now proceed to describe the theoretical framework for

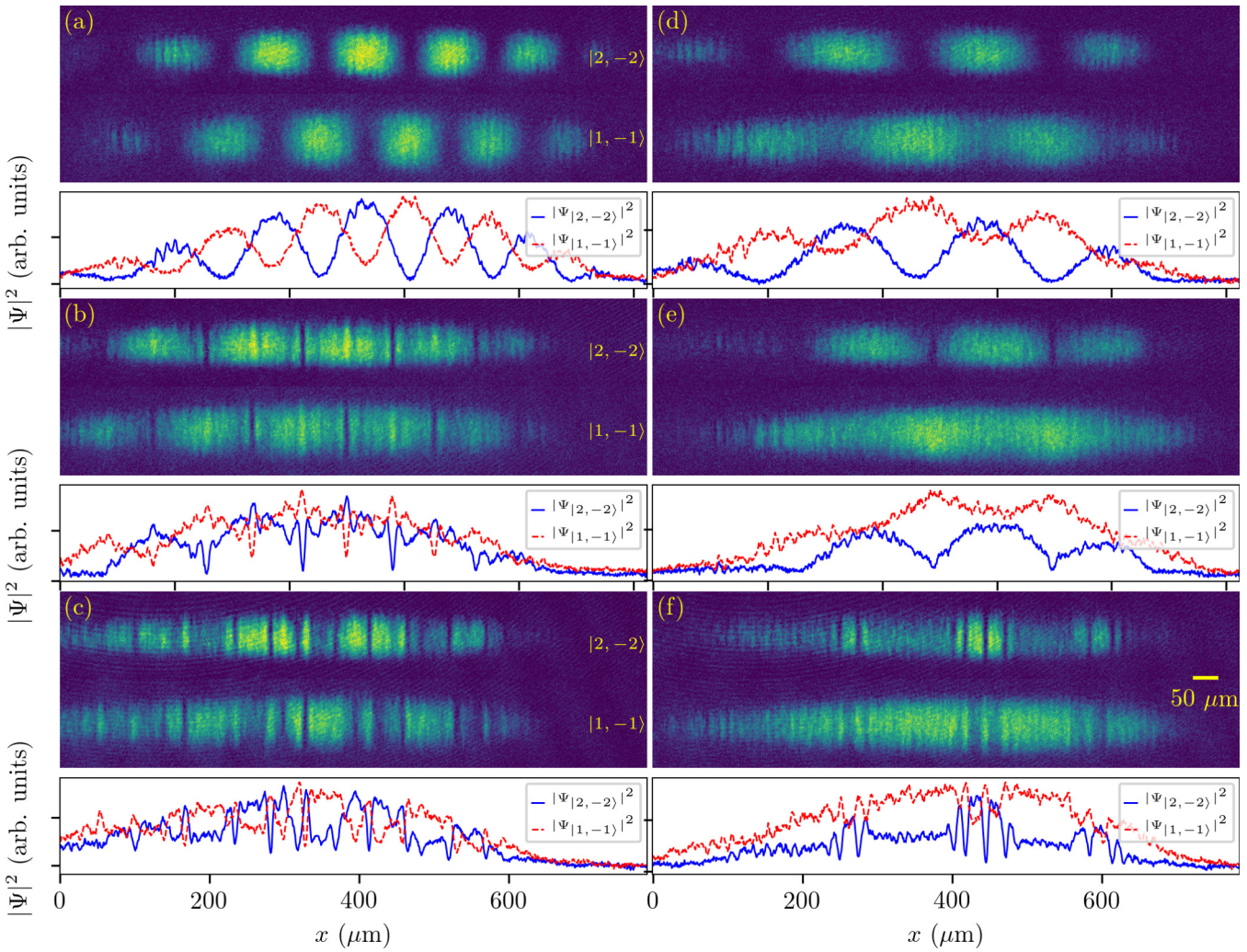

FIG. 1. Absorption images of the elongated BEC after Rabi winding with (a)–(c) near-zero detuning and (d)–(f) a detuning of $\delta = 2\pi \times 11$ kHz. A dual-imaging procedure places the $|2,-2\rangle$ atoms above the $|1,-1\rangle$ atoms for each measurement. The images (a) and (d) are taken after 15 ms of MW driving, (b) and (e) after an additional 150 ms of undriven evolution, and (c) and (f) after 410 ms. The corresponding integrated cross sections of each of the two components are shown for each panel.

modeling these solitonic configurations. We consider a binary mixture of repulsively interacting BECs composed of the two hyperfine states mentioned in the previous section, namely, $|F = 1, m_F = -1\rangle$ and $|F = 2, m_F = -2\rangle$, of ^{87}Rb [42] being confined in a one-dimensional (1D) harmonic oscillator potential. Such a cigar-shaped geometry can be realized experimentally [25,27,29] in a highly anisotropic trap with the longitudinal and transverse trapping frequencies obeying $\omega_x \ll \omega_\perp$, as described in Sec. II. Within mean-field theory, the dynamics of this binary mixture can be well approximated by the following system of coupled Gross-Pitaevskii equations (GPE) of motion [2–4]:

$$i\hbar\partial_t\psi_j = \left[-\frac{\hbar^2}{2m}\partial_x^2 + V(x) - \mu_j + \sum_{k=1}^{2} g_{jk}|\psi_k|^2\right]\psi_j. \quad (2)$$

In the above expression, $\psi_j(x,t)$ $(j = A, B)$ denotes the wave function for the $A \equiv |1,-1\rangle$ and $B \equiv |2,-2\rangle$ hyperfine states, respectively, and g_{jk} is the interaction coefficient between species j and k. Note here that in this framework, we do not consider particle transfer between the components of the mixture since they lie in a different spin manifold and therefore such processes are negligible, as has also been confirmed experimentally. Each $\psi_j(x,t)$ is normalized to the corresponding number of atoms, i.e., $N_j = \int_{-\infty}^{+\infty} |\psi_j|^2 dx$. Also, $m_A = m_B = m$ and μ_j refer to the atomic mass and chemical potentials for each of the species, respectively. The effective 1D coupling constants are given by $g_{jk} = 2\hbar\omega_\perp a_{jk}$, where a_{jk} are the three s-wave scattering lengths (with $a_{AB} = a_{BA}$) accounting for collisions between atoms that belong to the same (a_{jj}) or different $(a_{jk}, j \neq k)$ species. We note that both the intra- and interspecies scattering lengths can, in principle, be manipulated experimentally by means of Feshbach [43,44] or confinement-induced resonances [45,46]. Finally, $V(x)$ represents the external trapping potential.

For the numerical analysis presented below, we express the system of Eqs. (2) in the following dimensionless form:

$$i\frac{\partial\psi_A}{\partial t} = \left[-\frac{1}{2}\frac{\partial^2}{\partial x^2} + V + g_{AA}|\psi_A|^2 + g_{AB}|\psi_B|^2 - \mu_A\right]\psi_A, \tag{3}$$

$$i\frac{\partial\psi_B}{\partial t} = \left[-\frac{1}{2}\frac{\partial^2}{\partial x^2} + V + g_{BB}|\psi_B|^2 + g_{AB}|\psi_A|^2 - \mu_B\right]\psi_B. \tag{4}$$

Here, μ_i is the chemical potential of the ith species and $V(x) = \frac{1}{2}\omega_1^2 x^2$ is the dimensionless harmonic trapping potential with $\omega_A = \omega_B \equiv \omega_1 = \omega_x/\omega_\perp = 0.1$. Similar results can be found for much more elongated condensates with trap ratios $\omega_1 = 0.01$ closer to the one of the above reported experiments. For the numerical findings to be presented below, we fix the inter- and intraspecies interaction coefficients to the experimentally relevant values of the hyperfine states of ^{87}Rb, namely, $g_{AA} = 1.004$ and $g_{BB} = 0.9898$. To show the formation and variation of the DAD structures of interest, we first examine the relevant solutions as a function of g_{AB}, and then focus on parameter values that are proximal to the experimental ones. In the dimensionless units adopted above densities $|\psi_i|^2$, length, energy, and time are measured in units of $2a_{AA}$, $\sqrt{\frac{\hbar}{m\omega_\perp}}$, $\hbar\omega_\perp$, and $\omega_\perp^{-1}$, respectively.

For all of our numerical investigations, a fixed-point numerical iteration scheme is employed [47] in order to obtain bound states consisting of multiple DADs. To simulate the dynamical evolution of the DAD arrays governed by Eqs. (3) and (4), a fourth-order Runge-Kutta integrator is employed and a second-order finite-difference method is used for the spatial derivatives. The spatial and temporal discretization spacings are chosen as $dx = 0.05$ and $dt = 0.001$, respectively. Moreover, our numerical computations are restricted to a finite region by employing hard-wall boundary conditions. Particularly, in the dimensionless units adopted herein, the hard walls are located at $x_\pm = \pm 80$ and we do not observe any appreciable density for $|x| > 30$.

IV. SORTED DARK-ANTIDARK SOLITONS: STABILITY ANALYSIS AND DYNAMICS

In the following, we will explore the stability of bound states consisting of an arbitrary number of dark solitons in the first component of the mixture and corresponding antidark ones within the second component of the binary system of Eqs. (3) and (4). These configurations with all bright (or antidark) solitonic features in one component and all dark solitonic features in the other component will be referred to in the following as sorted DAD arrays. We remark that bound states composed of alternating dark and antidark entities within the same component cannot exist as stationary configurations; see, also, Sec. V. While such alternating states can (and do) emerge through the experimental procedure used in Sec. II, nevertheless they correspond to dynamically evolving (rather than stationary) states of the system.

In order to obtain the sorted stationary states, a tanh-shaped profile is used as an initial ansatz for the wave function with

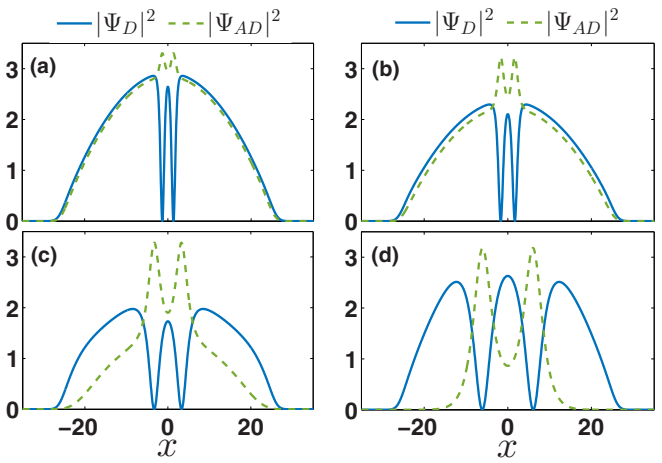

FIG. 2. Stationary states of two sorted DAD configurations for interspecies couplings (a) $g_{AB} = 0.2$, (b) $g_{AB} = 0.5$, (c) $g_{AB} = 0.9$, and (d) $g_{AB} = 0.98$. The densities $|\Psi_D|^2$ of the dark and $|\Psi_{AD}|^2$ of the antidark solitons are illustrated (see legend). In all cases, the states remain stable for long evolution times up to $t = 10^4$. Other parameters correspond to $\omega_1 = 0.1$, $g_{AA} = 1.004$, $g_{BB} = 0.9898$, $\mu_A = 3.5$, and $\mu_B = 3.4$. Note that all quantities shown are in dimensionless units.

n_S dark solitons that reads

$$\Psi_D = A(x)\prod_{j=1}^{n_S}\tanh\left[D\left(x - x_{0_j}\right)\right]. \tag{5}$$

In the above expression, $A(x) = (1/\sqrt{g_{AA}})\sqrt{\mu_A - V(x)}$ is the common Thomas-Fermi background into which the dark solitons are embedded. Additionally, D and x_{0_j} refer to the common inverse width and the center of the jth dark soliton, respectively. The ansatz employed for the initial-guess wave function of the corresponding antidark states is

$$\Psi_{AD} = \sum_{j=1}^{n_S} B(x) + C\,\mathrm{sech}\left[D\left(x - x_{0_j}\right)\right], \tag{6}$$

where the relevant background here is given by $B(x) = (1/\sqrt{g_{BB}})\sqrt{\mu_B - V(x)}$, and C denotes the amplitude of the density peak (on top of the background). Recall that DAD states consist of a density hump modeled here by a bright soliton as in the second term of Eq. (6) on top of the BEC background [34,48–51]. Utilizing the above ansatz, stationary states consisting of an arbitrary number of sorted DAD solitons symmetrically placed around the origin ($x = 0$) have been identified.

A. Two sorted DADs

Prototypical examples for states with two sorted DADs are shown in Fig. 2. Here, we see how the relevant state changes upon variation of the intercomponent interaction coefficient g_{AB}. The two-dark solitons that are well known to form a bound state in single-component BECs [4,7] now produce an attractive potential (due to the repulsive nature of the interaction and the absence of atoms in the dark solitons) for the second component. Thus, in this potential well, atoms

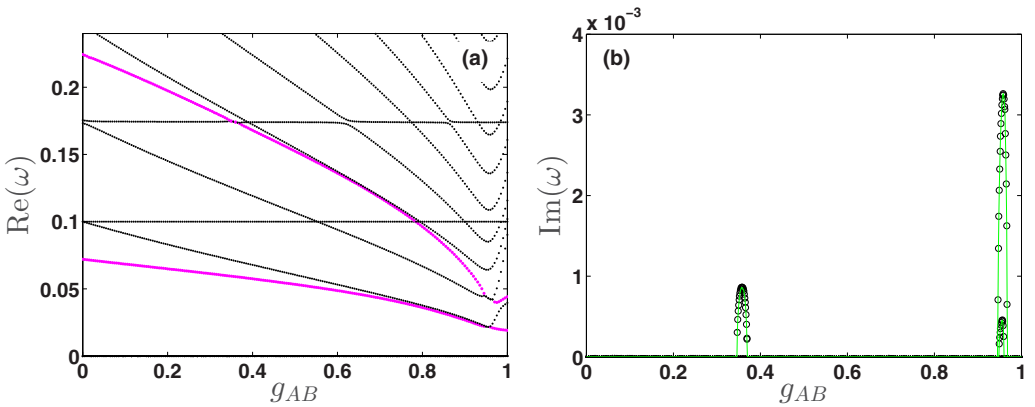

FIG. 3. BdG spectrum of a stationary state composed of two sorted DAD solitons as a function of the interspecies interaction strength g_{AB}. (a) The real part $\mathrm{Re}(\omega)$ and (b) the imaginary part $\mathrm{Im}(\omega)$ of the underlying eigenfrequencies is shown as a function of g_{AB}. In (a), the trajectories of the two anomalous modes appearing in the spectrum are denoted by magenta (light grey) dots. Note also that each point of the line $\mathrm{Re}(\omega) = 0$ is quadruple degenerate due to particle-number conservation per component, while the existence of a finite imaginary part signals the presence of an instability of the two-DAD configuration that occurs for $g_{AB} \in [0.347, 0.369]$ and $[0.946, 0.967]$. The solid lines in (b) provide a guide to the eye for each of the bifurcation loops appearing in the imaginary part of the eigenfrequencies. Other system parameters correspond to $\omega_1 = 0.1$, $\mu_A = 3.5$, $\mu_B = 3.4$, $g_{AA} = 1.004$, and $g_{BB} = 0.9898$, while all quantities depicted herein are in dimensionless units.

are trapped on top of the background state of the second component, generating antidark states. As g_{AB} is gradually increased, these states progress towards the immiscible limit and eventually, in the vicinity of the latter threshold, "isolate" themselves into bright-soliton-like droplets. Indeed, as the immiscibility threshold is crossed, the second component only prefers to localize itself in these bright structures, suggesting a morphing of the multi-DAD states into multi-DB ones.

To assess the stability of the aforementioned stationary DAD states, we perform a Bogoliubov–de Gennes (BdG) analysis, linearizing around the equilibrium as follows:

$$\Psi_D = \Psi_D^{(eq)} + \left[a(x)e^{-i\omega t} + b^\star(x)e^{i\omega^\star t}\right], \tag{7}$$

$$\Psi_{AD} = \Psi_{AD}^{(eq)} + \left[c(x)e^{-i\omega t} + d^\star(x)e^{i\omega^\star t}\right]. \tag{8}$$

The resulting linearization system for the eigenfrequencies ω (or, equivalently, eigenvalues $\lambda = i\omega$) and eigenfunctions $(a, b, c, d)^T$ is solved numerically. If modes with purely real eigenvalues (genuinely imaginary eigenfrequencies) or complex eigenvalues (eigenfrequencies) are identified, these are tantamount to the existence of an instability [14]. Indeed, upon our systematic variation of g_{AB} as discussed above (which, for suitable atomic species, is experimentally realizable via the use of Feshbach resonances), we identify such instabilities. While the two-DAD state is dynamically stable for a wide range of parametric values, there exist narrow intervals of g_{AB} (mentioned in the caption of Fig. 3) for which the solution is predicted to be unstable.

This suggests the relevance of a further effort in order to identify the modes responsible for the existence of the instability. We note that in addition to four modes in the spectrum at $\lambda = \omega = 0$ due to symmetries, namely, the conservations of the particle numbers in each component of the mixture, there are additional modes of interest that are referred to as anomalous or negative-energy ones [52]. These are modes highlighting the excited nature of the state under consideration (i.e., for the ground state there are no such modes). These eigenstates are quantified via the so-called negative-energy or negative Krein signature [52]. The mode energy (or Krein signature) is defined as

$$K = \omega_1 \int \left(|a|^2 - |b|^2 + |c|^2 - |d|^2\right)dx, \tag{9}$$

in a multicomponent system such as the one considered herein. An example of this sort is shown in the BdG spectrum presented in the left panel of Fig. 3 for the two sorted DAD configurations, where the negative-energy modes are denoted by magenta dots.

The existence and parametric variation of such modes is of particular relevance since their collision with opposite (positive) Krein signature modes gives rise to stability changes in the form of oscillatory instabilities or Hamiltonian-Hopf bifurcations [4,52]. Indeed, what is happening here, along the axis of real eigenfrequencies, is that modes with $K > 0$ and $K < 0$ collide in pairs and give rise to complex eigenfrequency quartets, as we will observe below. These resulting complex eigenfrequencies (all four of them) have $K = 0$ until they "complete" an oscillatory instability "bubble." Then, these eigenmodes "land back" on the real eigenfrequency axis and retrieve their respective $K < 0$ or $K > 0$ traits. The resulting instability is the one that we will trace later on in the dynamics as well. Our calculations show that there are *two* such modes in the system consisting of two sorted DAD solitons. Additionally, *three* and *six* such modes appear when considering, respectively, the three- and the six-DAD soliton configuration; see, e.g., Figs. 7 and 10. This is in agreement with the case of dark solitons in single-component BECs, where an N-soliton state has been shown to possess N negative-energy modes [53]. Specifically, for all the distinct sorted DAD configurations investigated herein, there exist intervals where the above-identified anomalous modes collide with $K > 0$ modes pertaining to the collective excitations of the background condensate. For instance, such a collisional interval occurs for $g_{AB} \in [0.946, 0.967]$ for the two-DAD configuration [Fig. 3(a)], while for the three- and six-DAD states,

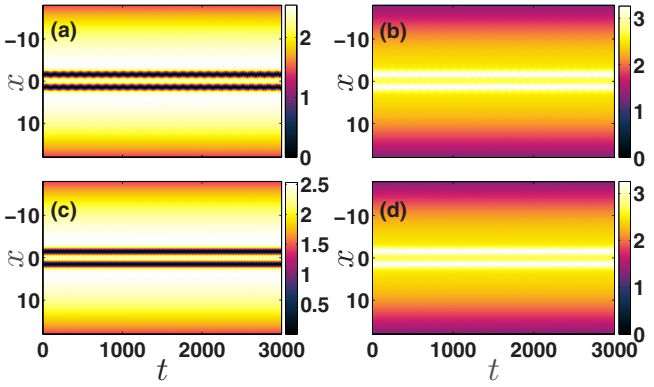

FIG. 4. Dynamical evolution of a stationary state of two sorted DAD solitons. (a), (c) [(b), (d)] The evolution of the dark [antidark] soliton component upon adding the eigenvectors of the (a), (b) first and the (c), (d) second anomalous mode identified in the BdG spectrum of Fig. 3. Other system parameters correspond to $\mu_A = 3.5$, $\mu_B = 3.4$, $g_{AA} = 1.004$, $g_{BB} = 0.9898$, and $g_{AB} = 0.36$. All quantities plotted are in dimensionless units.

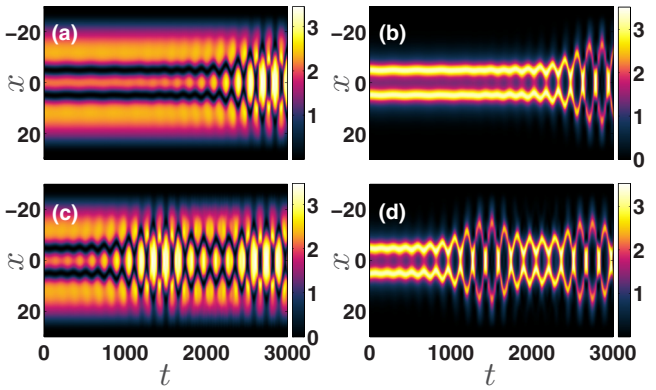

FIG. 5. Evolution of a stationary state of two sorted DAD solitons for $\mu_A = 3.5$. The time evolution of the dark [antidark] soliton components is presented in (a) and (c) [(b) and (d)] upon adding the eigenvectors of the (a), (b) first and the (c), (d) second anomalous mode identified in the BdG spectrum of Fig. 3. The remaining system parameters are $\mu_B = 3.4$, $g_{AA} = 1.004$, $g_{BB} = 0.9898$, and $g_{AB} = 0.96$. All quantities illustrated above are given in dimensionless units.

such intervals appear, e.g., for $g_{AB} \in [0.301, 0.342]$ [Fig. 7(a)] and for $g_{AB} \in [0.19, 0.25]$, respectively [Fig. 10(a)]. Notice also that within the aforementioned parameter intervals, whenever such collisions take place a bifurcation occurs in the corresponding imaginary part, presented in Figs. 3(b), 7(b), and 10(b), respectively, signaling the presence of an instability of the relevant DAD configuration in each case.

We now explore the direct numerical evolution of the two-DAD solitonic state for different parametric values. In Fig. 4, we offer an example for $g_{AB} = 0.36$ for which the relevant configuration is stable. We examine the dynamical outcome of the coherent structure when adding the first [Figs. 4(a) and 4(b)] and the second [Figs. 4(c) and 4(d)] anomalous mode to the wave. Close inspection indicates that the former lower-frequency mode leads to an in-phase oscillation of the two DAD structures, while the latter higher-frequency mode leads to an out-of-phase one. Nevertheless, both configurations turn out to be stable, in agreement with our stability analysis observations in Fig. 3. On the contrary, in Fig. 5, the higher-frequency anomalous mode associated with out-of-phase DAD solitary wave oscillations is unstable due to a resonant collision with one of the positive Krein signature modes. Consequently and irrespectively of whether we excite chiefly the first [Figs. 5(a) and 5(b)] or the second [Figs. 5(c) and 5(d)] anomalous mode, eventually an instability ensues. Naturally, in Figs. 5(c) and 5(d), where the responsible mode for the instability has been excited, the relevant phenomenology arises earlier. Nevertheless, it arises in both cases and leads to a resonant growth of the out-of-phase DAD waves' oscillation amplitude before leading to a saturation and, subsequently, to a recurrence effect [see, especially, Figs. 5(c) and 5(d)]. It is important to comment at this point that for larger g_{AB} values also, the lowest-lying anomalous mode destabilizes, resulting in the appearance of the inner loop present in Fig. 3(b). The associated instability window here occurs for $0.949 \leqslant g_{AB} \leqslant 0.959$. Notice, however, that the imaginary eigenfrequencies corresponding to this bifurcation are suppressed (i.e., of much smaller growth rate) when compared to the predominant ones of the outer bifurcation. This suggests that even though the lowest-lying mode destabilizes, it is not the one (principally) responsible for the observed instability of the two-DAD configuration. This is indeed confirmed by inspecting once more the dynamical evolution presented in Figs. 5(a) and 5(b).

B. Three sorted DADs

We now turn to a similar set of results for the configurations with three sorted DADs. In Fig. 6, we observe how the three solitary wave state progressively transforms itself

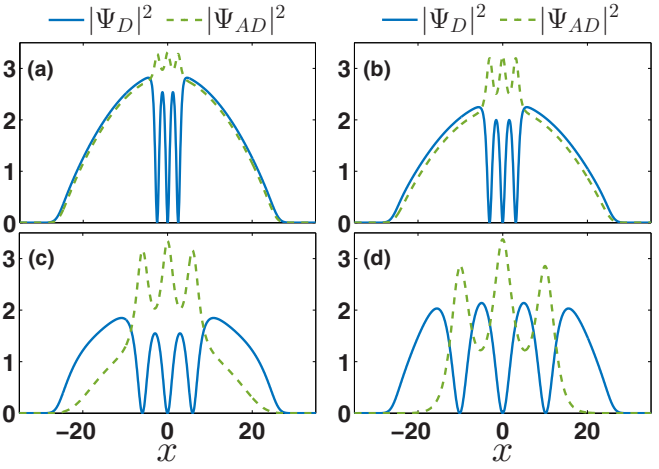

FIG. 6. Stationary states of three sorted DAD solitons for different interspecies interactions, namely, (a) $g_{AB} = 0.2$, (b) $g_{AB} = 0.5$, (c) $g_{AB} = 0.9$, and (d) $g_{AB} = 0.98$. The density of both the dark $|\Psi_D|^2$ and the antidark $|\Psi_{AD}|^2$ component is shown (see legend). The presented states remain stable for long evolution times up to $t = 10^4$. The remaining parameters of the system are $\omega_1 = 0.1$, $g_{AA} = 1.004$, $g_{BB} = 0.9898$, $\mu_A = 3.5$, and $\mu_B = 3.4$. All quantities shown are in dimensionless units.

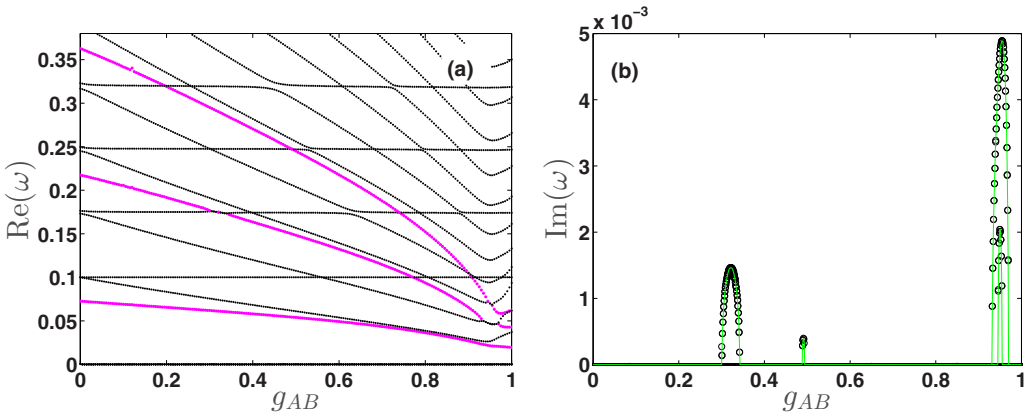

FIG. 7. BdG spectrum of a stationary state of three sorted DAD solitons with respect to the interspecies interaction strength g_{AB}. (a) Real part $\mathrm{Re}(\omega)$ of the underlying eigenfrequencies for varying g_{AB}. The points lying at $\mathrm{Re}(\omega) = 0$ are quadruple degenerate due to particle-number conservation in each component. Additionally, the trajectories of the three anomalous modes identified here are depicted by magenta (light grey) dots. (b) Imaginary part $\mathrm{Im}(\omega)$ of the eigenfrequencies. The corresponding instability windows of the three-DAD configuration are $0.301 \leqslant g_{AB} \leqslant 0.342$, $0.489 \leqslant g_{AB} \leqslant 0.493$, and $0.932 \leqslant g_{AB} \leqslant 0.969$. Solid lines in (b) provide a guide to the eye for each of the individual bifurcation loops emerging in the imaginary part of the eigenfrequencies. The remaining system parameters that are used correspond to $\omega_1 = 0.1$, $\mu_A = 3.5$, $\mu_B = 3.4$, $g_{AA} = 1.004$, and $g_{BB} = 0.9898$, while all quantities shown are given in dimensionless units.

(in its stationary form) as g_{AB} is increased. The prevailing picture at low g_{AB} once again involves the dark solitary waves forming wells where the antidark states of the second component are trapped. Gradually, as g_{AB} is increased, more of the second component density gets encompassed in the antidark states, which eventually (as the immiscibility threshold is approached) become essentially dropletlike and will separate into DB states for sufficiently large g_{AB}. As may be expected, the BdG spectrum now features three anomalous modes, as illustrated in Fig. 7. These, in turn, yield their own potential resonant intervals, as discussed in the caption of the associated figure. The lowest of these modes is again an in-phase one, the second mode involves a quiescent central DAD, while the outer ones oscillate out of phase; finally, the third mode involves an in-phase oscillation of the outer waves and an out-of-phase one of the middle wave. The first mode is never resonant in the parametric regime that is considered. The second mode causes the first instability window and is principally responsible for the third window (where it is associated with the highest growth rate), while the third mode causes the second instability window and also leads to a partial destabilization within the third window. Focusing our attention on the predominant third bifurcation interval (associated with the maximal instability growth rate) present for the three-DAD configuration [Fig. 7(b)], we next examine the unstable dynamics associated with it. Notice that as in the investigation of configurations with two DADs, here an inner loop appears in the respective BdG spectrum [Fig. 7(b)], suggesting in this case the destabilization of not only the second, but also the third anomalous mode for values of g_{AB} lying in the interval $0.946 \leqslant g_{AB} \leqslant 0.954$. However, in Fig. 8, we can observe that independent of which of the modes we add to the initial stationary configuration with three DADs, the resonant second mode will eventually be excited, giving rise to the growth of the associated configuration involving the out-of-phase motion of the outer DADs, while the middle one remains quiescent. The saturation of the relevant growing oscillation and the recurrence of the phenomenon are clearly observed, especially in Figs. 8(c) and 8(d), where the unstable mode was added initially to the stationary state and hence gave rise to the associated instability earlier.

C. Six sorted DADs

In order to generalize our findings to even larger DAD soliton arrays, we now consider the stability properties of a stationary state consisting of six sorted DAD solitons. The gradual transformation of the obtained stationary states as g_{AB} increases is illustrated in Figs. 9(a)–9(d). One can see in the figure how the blobs corresponding to the location of the individual DADs separate as g_{AB} is increased. To address the stability of these bound states, we employ the

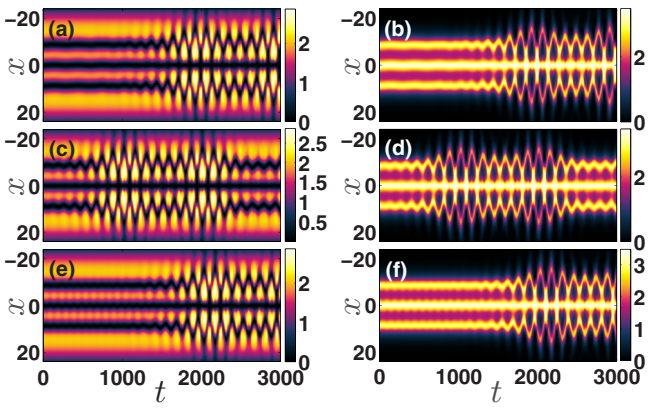

FIG. 8. Dynamical evolution of three sorted DAD solitons. (a), (c), (e) [(b), (d), (f)] The evolution of the dark [antidark] soliton component upon adding, respectively, the eigenvectors corresponding to the (a), (b) first, (c), (d) second, and (e), (f) third anomalous mode identified in the BdG spectrum of Fig. 7. The remaining system parameters correspond to $\mu_A = 3.5$, $\mu_B = 3.4$, $g_{AA} = 1.004$, $g_{BB} = 0.9898$, and $g_{AB} = 0.96$. The quantities shown are in dimensionless units.

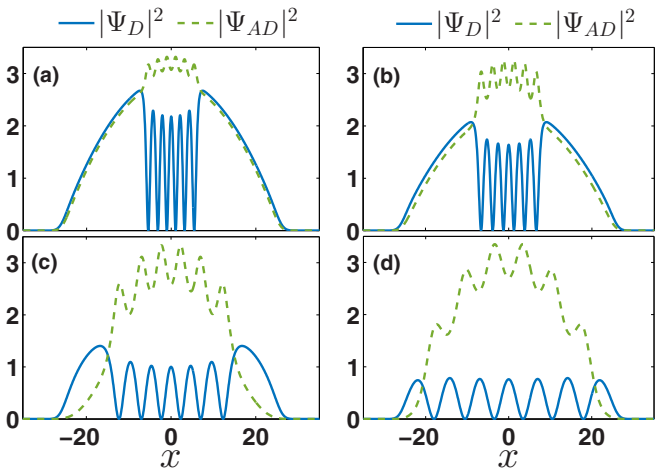

FIG. 9. Stationary states consisting of six sorted DAD solitons for different interspecies interactions, namely, (a) $g_{AB} = 0.2$, (b) $g_{AB} = 0.5$, (c) $g_{AB} = 0.9$, and (d) $g_{AB} = 0.98$. The densities $|\Psi_D|^2$ of the dark and $|\Psi_{AD}|^2$ of the antidark components are shown (see legend). The remaining system parameters are $\omega_1 = 0.1$, $g_{AA} = 1.004$, $g_{BB} = 0.9898$, $\mu_A = 3.5$, and $\mu_B = 3.4$, while all quantities shown are in dimensionless units.

same diagnostics as in the previous two cases. Specifically, for the numerical findings to be presented below, we fix $\mu_A = 3.5$, $\mu_B = 3.4$ and we vary g_{AB} within the interval [0, 1]. The relevant BdG spectrum is illustrated in Figs. 10(a) and 10(b). Once again, the magenta dots are used to denote the anomalous (negative Krein signature) modes in the figure. Importantly, a cascade of Hamiltonian-Hopf bifurcations can be observed in this BdG spectrum as is corroborated by the finite imaginary eigenfrequencies (or instability growth rates), $\mathrm{Im}(\omega)$, depicted in Fig. 10(b). The associated instability intervals, five in this case, are indicated in the figure caption.

The corresponding modes are simply the normal modes of vibration of the six solitary waves considered as particles. In that vein, the lowest out of the six anomalous modes present for the state with six DADs is an in-phase one. Accordingly, the highest, i.e., the sixth, anomalous mode involves an out-of-phase motion of adjacent coherent structures. Finally, all the intermediate modes, i.e., from the second until the fifth one, entail relevant mixed phase oscillations. Turning to the fifth interval, exhibiting the largest instability growth rate, as illustrated in Fig. 10(b), we next inspect the unstable dynamics of the six-DAD configuration for $g_{AB} = 0.94$ (Fig. 11). Before delving into the details of the associated dynamics, it is important to stress at this point that as the immiscibility threshold is approached, four out of the six anomalous modes destabilize. This can be observed by close inspection of the spectrum, revealing four loops in the imaginary part of the BdG spectrum in Fig. 10(b). Two possible manifestations of the instability, using perturbations along the third and sixth eigenmode, are shown in Fig. 11. Specifically, upon adding the third of the aforementioned modes to the initially stationary six-DAD state [Figs. 11(a) and 11(b)], we observe that the instability manifests itself from the very early stages of the dynamics, leading to the oscillatory motion of the six-DAD configuration, involving the in-phase oscillation of the central and the outermost DAD waves. The intermediate pair of DADs remains approximately quiescent during this oscillatory dynamical evolution. However, for all the remaining cases, it is found that independently of which mode we add to the initially stationary six-DAD state, namely, either the first, second, fourth, fifth, or sixth mode [see here Figs. 11(c) and 11(d)], the resonant second mode will eventually be excited, giving rise to a growth of the corresponding configuration that entails the out-of-phase vibration of the central DAD waves and the in-phase oscillation between the second and the outermost DAD pairs.

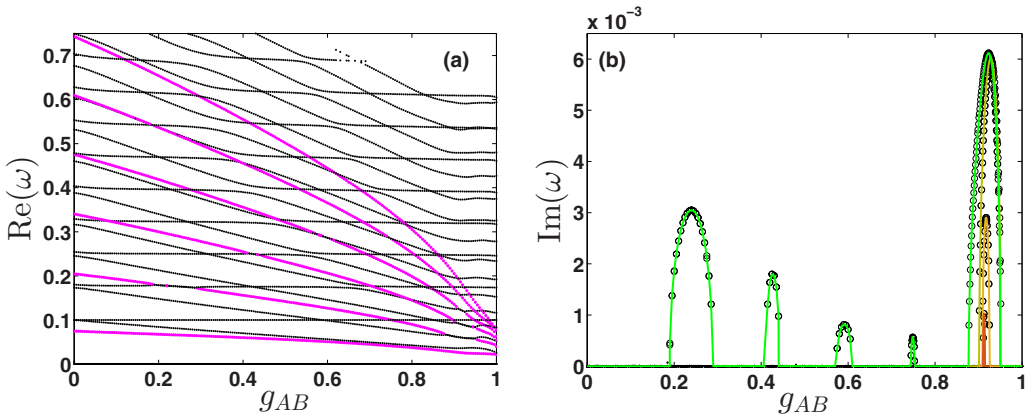

FIG. 10. BdG spectrum of a stationary state consisting of six sorted DAD solitons. The trajectories of six anomalous modes can be inferred in (a), denoted by magenta (light grey) dots. All points residing at $\mathrm{Re}(\omega) = 0$ exhibit a quadruple degeneracy stemming from the particle-number conservation of each component. Additionally, a cascade of bifurcations occurs, as g_{AB} is varied, in this BdG spectrum as is evident by the finite imaginary eigenfrequencies shown in (b). The associated instability intervals, being denoted by the black circles, are $0.19 \leqslant g_{AB} \leqslant 0.285$, $0.415 \leqslant g_{AB} \leqslant 0.44$, $0.575 \leqslant g_{AB} \leqslant 0.605$, $0.745 \leqslant g_{AB} \leqslant 0.752$, and $0.878 \leqslant g_{AB} \leqslant 0.951$. Solid lines shown in (b) provide a guide to the eye for the individual bifurcation loops appearing in the imaginary part of the eigenfrequencies. Other parameters used are $\mu_A = 3.5$, $\mu_B = 3.4$, $g_{AA} = 1.004$, and $g_{BB} = 0.9898$. All quantities shown are provided in dimensionless units.

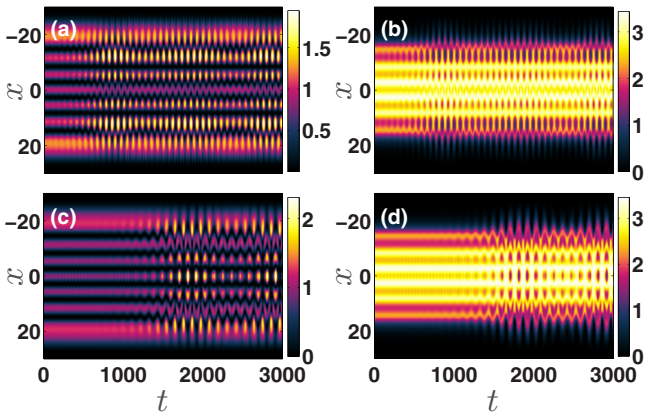

FIG. 11. Evolution of a stationary state of six sorted DAD solitary waves for $\mu_A = 3.5$. The time evolution of the dark [antidark] soliton component is presented in (a) and (c) [(b) and (d)] upon adding the eigenvectors of the (a), (b) third and the (c), (d) sixth anomalous mode identified in the BdG spectrum of Fig. 10. The remaining system parameters are $\mu_B = 3.4$, $g_{AA} = 1.004$, $g_{BB} = 0.9898$, and $g_{AB} = 0.94$, with all quantities shown being in dimensionless units.

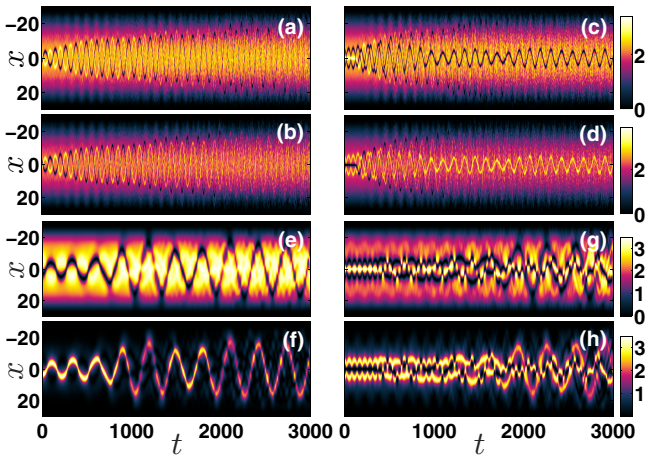

FIG. 12. Spatiotemporal evolution of the densities of both components showcasing the oscillations and interactions of alternating DAD solitons for (a)–(d) $g_{AB} = 0.6$ and (e)–(h) $g_{AB} = 0.96$, respectively. (a), (e) [(c), (g)] An initial seeding of a single dark [two darks] and a single antidark in the first component and (b), (f) [(d), (h)] their relevant mirror images in the second component. Other parameters used are $\mu_A = 3.5$, $\mu_B = 3.4$, $g_{AA} = 1.004$, and $g_{BB} = 0.9898$. The quantities illustrated are in dimensionless units.

V. ALTERNATING DARK-ANTIDARK SOLITONS

Having discussed the static properties of arrays consisting of multiple sorted DAD solitons, motivated by the experimental observations we next turn our attention to the dynamics of solitonic states consisting of dark and antidark waves in each of the components of the mixture in an alternating fashion. Despite our extensive efforts to identify stationary states consisting of alternating dark and antidark solitons (i.e., DAD configurations where the dark features and, in a complementary way, the antidark features alternate between the two pseudospin components), our numerical findings suggest that such a state cannot be stationary. We have dynamically constructed such alternating states and monitored their evolution and interactions [Figs. 12(a)–12(h)]. Examples illustrating the spatiotemporal evolution of solitonic entities composed, for instance, of one dark followed by an antidark soliton in the first component, and vice versa in the second component, are presented in Figs. 12(a), and 12(b) for $g_{AB} = 0.6$ and in Figs. 12(e), and 12(f) for $g_{AB} = 0.96$ respectively. Notice that regardless of the value of the intercomponent coupling strength, the alternating entities perform oscillations of growing amplitude during the initial stages of the dynamics. However, for smaller values of g_{AB} and for times around $t \approx 2 \times 10^3$, the alternating states are lost within the significantly excited background and only a single DAD soliton appears to survive at later times. On the other hand, a distinct evolution possibility arises as g_{AB} increases. For instance, for $g_{AB} = 0.96$ and focusing on these later times, beating dark-dark solitons develop in the two components and propagate within the BEC medium for (dimensionless) times up to $t \sim 3 \times 10^3$ that we have considered [31].

A similar outcome (i.e., involving the unstable dynamics) arises upon increasing the number of alternating waves in each component. Specifically, and as depicted in Figs. 12(c), and 12(g) [Figs. 12(d), and 12(h)], when two dark [antidark] and a central antidark [dark] solitary waves are initialized in the first [second] hyperfine state, a nearly bound state formation occurs in the relevant dynamics. Here, the central wave in each component oscillates in its amplitude persistently at the center of the configuration, while the outer two waves perform out-of-phase oscillations. However, at later times, i.e., around $t \approx 200$ for $g_{AB} = 0.6$ and around $t \approx 500$ for $g_{AB} = 0.96$, the alternating structures are set in motion, resulting, in turn, in a single sorted DAD soliton oscillating around the trap center for all times in the former case, and oscillating and interacting beating dark-dark entities for the latter scenario.

It is also worth commenting at this point that since the alternating states are not stationary ones, emission of radiation from the relevant pattern takes place right after the initial (at $t = 0$) seeding, resulting in an excited BEC background in all cases studied here. Finally, we note in passing that one can systematically study the dynamical evolution of the system when considering an arbitrarily large number of alternating dark and antidark waves. Here, more complex interactions between the ensuing waves take place, including their deformation into beating dark-dark solitons (results not shown here).

VI. CONCLUSIONS

In the present work, we have been motivated by experimental realizations of two-component BECs in an elongated trap to consider solitary wave structures involving dark solitonic states in one of the components and corresponding antidark ones in the other. The combination of a spatially dependent Zeeman shift with a uniform fixed-frequency microwave drive was demonstrated as a viable experimental pathway to the formation of such structures. It was possible to create experimentally both cases where all the dark solitons were in one component and the antidark ones in the other, as well as settings where in each component the dark and antidark

waves alternate. We corroborated these experimental realizations with a theoretical analysis based on a two-component Gross-Pitaevskii model in a quasi-one-dimensional geometry. We saw that such a setup enables the formulation of stationary configurations with all the dark solitary waves in one component and the antidark ones in the other component. In fact, we found such states with two, three, six, and, in principle, arbitrary "lattices" of dark waves in one component and antidarks in the other. On the other hand, this was not the case for the alternating dark-antidark configurations. Such a state could only be traced as a dynamical one and never as a stationary one. For the multiple sorted DAD wave case, we found that the waves were generally dynamically stable, although the presence of N anomalous modes (in the states with N DAD waves) could potentially lead to windows of oscillatory instabilities. The latter were observed to give rise to resonant growth of the oscillations involving the DAD waves, but eventually a saturation thereof and a potential recurrence subsequently of the associated dynamics.

Naturally, there are many possible extensions of this direction of studies. From an analytical standpoint, it is relevant to extend the type of understanding that exists for the interactions of dark [7] and even dark-bright [4,54] solitary waves to the realm of dark-antidark structures. This will provide a guideline for understanding the formation of equilibria (when all the darks are in the same component) or the absence thereof (when the adjacent darks are in alternating components). Another direction that would be of substantial interest would be to extend relevant structures to the realm of spinor condensates with three spin states where it is possible to envision different types of extensions, e.g., ones where two components are dark and one antidark, as well as ones where only one component is dark and two are antidark [55]. Finally, it is also natural to extend considerations to higher dimensions and seek lattices of multiple vortex-antidark states either with the vortices bearing the same or alternating topological charges. Understanding in a quantitative fashion the interaction of two such states or the formation of lattices of more such states is also a topic of ongoing interest [56]. Studies along these directions are presently underway and will be reported in future publications.

ACKNOWLEDGMENTS

P.G.K. is grateful to the Leverhulme Trust and to the Alexander von Humboldt Foundation for support and to the Mathematical Institute of the University of Oxford for its hospitality. This material is based upon work supported by the U.S. National Science Foundation under Grants No. PHY-1602994 and No. DMS-1809074 (P.G.K.). G.C.K., S.I.M., and P.S. gratefully acknowledge financial support by the Deutsche Forschungsgemeinschaft (DFG) in the framework of the SFB 925 "Light induced dynamics and control of correlated quantum systems". S.I.M. gratefully acknowledges financial support in the framework of the Lenz-Ising Award of the University of Hamburg. T.M.B., S.M.M., M.K.H.O., and P.E. acknowledge funding from the NSF under Grants No. PHY-1607495 and No. PHY-1912540.

[1] C. J. Pethick and H. Smith, *Bose-Einstein Condensation in Dilute Gases* (Cambridge University Press, Cambridge, 2002).
[2] L. P. Pitaevskii and S. Stringari, *Bose-Einstein Condensation* (Oxford University Press, Oxford, 2003).
[3] *Emergent Nonlinear Phenomena in Bose-Einstein Condensates. Theory and Experiment*, edited by P. G. Kevrekidis, D. J. Frantzeskakis, and R. Carretero-González (Springer-Verlag, Berlin, 2008).
[4] P. G. Kevrekidis, D. J. Frantzeskakis, and R. Carretero-González, *The Defocusing Nonlinear Schrödinger Equation* (SIAM, Philadelphia, 2015).
[5] Yu. S. Kivshar and G. P. Agrawal, *Optical Solitons: From Fibers to Photonic Crystals* (Academic Press, San Diego, 2003).
[6] M. J. Ablowitz, *Nonlinear Dispersive Waves* (Cambridge University Press, Cambridge, 2011).
[7] D. J. Frantzeskakis, J. Phys. A **43**, 213001 (2010).
[8] A. L. Fetter and A. A. Svidzinksy, J. Phys.: Condens. Matter **13**, R135 (2001).
[9] A. L. Fetter, Rev. Mod. Phys. **81**, 647 (2009).
[10] S. Komineas, Eur. Phys. J.: Spec. Top. **147**, 133 (2007).
[11] Y. V. Kartashov, B. A. Malomed, Ya. Shnir, and L. Torner, Phys. Rev. Lett. **113**, 264101 (2014).
[12] D. Proment, M. Onorato, and C. F. Barenghi, Phys. Rev. E **85**, 036306 (2012).
[13] C. Ticknor, V. P. Ruban, and P. G. Kevrekidis, Phys. Rev. A **99**, 063604 (2019).
[14] P. G. Kevrekidis and D. J. Frantzeskakis, Rev. Phys. **1**, 140 (2016).
[15] D. N. Christodoulides, Phys. Lett. A **132**, 451 (1988).
[16] V. V. Afanasyev, Yu. S. Kivshar, V. V. Konotop, and V. N. Serkin, Opt. Lett. **14**, 805 (1989).
[17] Yu. S. Kivshar and S. K. Turitsyn, Opt. Lett. **18**, 337–339 (1993).
[18] R. Radhakrishnan and M. Lakshmanan, J. Phys. A: Math. Gen. **28**, 2683 (1995).
[19] A. V. Buryak, Yu. S. Kivshar, and D. F. Parker, Phys. Lett. A **215**, 57 (1996).
[20] A. P. Sheppard and Yu. S. Kivshar, Phys. Rev. E **55**, 4773 (1997).
[21] Q.-Han Park and H. J. Shin, Phys. Rev. E **61**, 3093 (2000).
[22] Z. Chen, M. Segev, T. H. Coskun, D. N. Christodoulides, and Yu. S. Kivshar, J. Opt. Soc. Am. B **14**, 3066 (1997).
[23] E. A. Ostrovskaya, Yu. S. Kivshar, Z. Chen, and M. Segev, Opt. Lett. **24**, 327 (1999).
[24] Th. Busch and J. R. Anglin, Phys. Rev. Lett. **87**, 010401 (2001).
[25] C. Becker, S. Stellmer, P. Soltan-Panahi, S. Dörscher, M. Baumert, E.-M. Richter, J. Kronjäger, K. Bongs, and K. Sengstock, Nat. Phys. **4**, 496 (2008).
[26] C. Hamner, J. J. Chang, P. Engels, and M. A. Hoefer, Phys. Rev. Lett. **106**, 065302 (2011).
[27] S. Middelkamp, J. J. Chang, C. Hamner, R. Carretero-González, P. G. Kevrekidis, V. Achilleos, D. J. Frantzeskakis, P. Schmelcher, and P. Engels, Phys. Lett. A **375**, 642 (2011).
[28] D. Yan, J. J. Chang, C. Hamner, P. G. Kevrekidis, P. Engels, V. Achilleos, D. J. Frantzeskakis, R. Carretero-González, and P. Schmelcher, Phys. Rev. A **84**, 053630 (2011).

[29] M. A. Hoefer, J. J. Chang, C. Hamner, and P. Engels, Phys. Rev. A **84**, 041605(R) (2011).
[30] D. Yan, J. J. Chang, C. Hamner, M. Hoefer, P. G. Kevrekidis, P. Engels, V. Achilleos, D. J. Frantzeskakis, and J. Cuevas, J. Phys. B: At. Mol. Opt. Phys. **45**, 115301 (2012).
[31] A. Álvarez, J. Cuevas, F. R. Romero, C. Hamner, J. J. Chang, P. Engels, P. G. Kevrekidis, and D. J. Frantzeskakis, J. Phys. B **46**, 065302 (2013).
[32] A. M. Kamchatnov, Y. V. Kartashov, P.-E. Larr é, and N. Pavloff, Phys. Rev. A **89**, 033618 (2014).
[33] C. Qu, L. P. Pitaevskii, and S. Stringari, Phys. Rev. Lett. **116**, 160402 (2016).
[34] I. Danaila, M. A. Khamehchi, V. Gokhroo, P. Engels, and P. G. Kevrekidis, Phys. Rev. A **94**, 053617 (2016).
[35] T. M. Bersano, V. Gokhroo, M. A. Khamehchi, J. D'Ambroise, D. J. Frantzeskakis, P. Engels, and P. G. Kevrekidis, Phys. Rev. Lett. **120**, 063202 (2018).
[36] X. Chai, D. Lao, K. Fujimoto, R. Hamazaki, M. Ueda, and C. Raman, Phys. Rev. Lett. **125**, 030402 (2020).
[37] W. Wang and P. G. Kevrekidis, Phys. Rev. E **91**, 032905 (2015).
[38] M. R. Matthews, B. P. Anderson, P. C. Haljan, D. S. Hall, M. J. Holland, J. E. Williams, C. E. Wieman, and E. A. Cornell, Phys. Rev. Lett. **83**, 3358 (1999).
[39] J. Williams, R. Walser, J. Cooper, E. A. Cornell, and M. Holland, Phys. Rev. A **61**, 033612 (2000).
[40] A. B. Deb, B. J. Sawyer, and N. Kjærgaard, Phys. Rev. A **88**, 063607 (2013).
[41] C. Hamner, Y. Zhang, J. J. Chang, C. Zhang, and P. Engels, Phys. Rev. Lett. **111**, 264101 (2013).
[42] M. Egorov, B. Opanchuk, P. Drummond, B. V. Hall, P. Hannaford, and A. I. Sidorov, Phys. Rev. A **87**, 053614 (2013).
[43] T. Köhler, K. Góral, and P. S. Julienne, Rev. Mod. Phys. **78**, 1311 (2006).
[44] C. Chin, R. Grimm, P. Julienne, and E. Tiesinga, Rev. Mod. Phys. **82**, 1225 (2010).
[45] M. Olshanii, Phys. Rev. Lett. **81**, 938 (1998).
[46] J. I. Kim, V. S. Melezhik, and P. Schmelcher, Phys. Rev. Lett. **97**, 193203 (2006).
[47] C. T. Kelley, *Solving Nonlinear Equations with Newton's Method* (Society for Industrial and Applied Mathematics, Philadelphia, 1995).
[48] P. G. Kevrekidis, H. E. Nistazakis, D. J. Frantzeskakis, B. A. Malomed, and R. Carretero-González, Eur. Phys. J. D **28**, 181 (2004).
[49] G. C. Katsimiga, G. M. Koutentakis, S. I. Mistakidis, P. G. Kevrekidis, and P. Schmelcher, New J. Phys. **19**, 073004 (2017).
[50] S. I. Mistakidis, G. C. Katsimiga, P. G. Kevrekidis, and P. Schmelcher, New J. Phys. **20**, 043052 (2018).
[51] H. Kiehn, S. I. Mistakidis, G. C. Katsimiga, and P. Schmelcher, Phys. Rev. A **100**, 023613 (2019).
[52] Dmitry V. Skryabin, Phys. Rev. A **63**, 013602 (2000).
[53] T. Kapitula and P. G. Kevrekidis, Chaos **15**, 037114 (2005).
[54] G. C. Katsimiga, J. Stockhofe, P. G. Kevrekidis, and P. Schmelcher, Phys. Rev. A **95**, 013621 (2017).
[55] C.-M. Schmied (private communication).
[56] K. Kasamatsu, M. Eto, and M. Nitta, Phys. Rev. A **93**, 013615 (2016).